Applied Catalysis B: Environmental 300 (2022) 120735

Contents lists available at ScienceDirect

Applied Catalysis B: Environmental

journal homepage: www.elsevier.com/locate/apcatb

Distinct photocatalytic charges separation pathway on CuO_x modified rutile and anatase TiO_2 under visible light

Min Chen [a], Jianhua Chen [b,c], Chuncheng Chen [b,c,*], Changbin Zhang [a,c,*], Hong He [a,c]

[a] State Key Joint Laboratory of Environment Simulation and Pollution Control, Research Center for Eco-Environment Sciences, Chinese Academy of Sciences, Beijing 100085, PR China
[b] Key Laboratory of Photochemistry, CAS Research/Education Center for Excellence in Molecular Sciences, Institute of Chemistry, Chinese Academy of Sciences, Beijing 100190, PR China
[c] University of Chinese Academy of Sciences, Beijing 100049, PR China

ARTICLE INFO

Keywords:
Anatase
Rutile
Cu
Charge migration

ABSTRACT

Modification of TiO_2 with copper oxides clusters (CuO_x-TiO_2) induces visible-light absorption and enhances its activity. In this work, we investigated the CuO_x-anatase and CuO_x-rutile for the photocatalytic oxidation of gaseous NH_3 under visible light. In contrast with the widely reported results that CuO_x-anatase displays higher performance than CuO_x-rutile in photocatalytic oxidation or reduction, we surprisingly observed that CuO_x-rutile is able to oxidize NH_3 efficiently under visible light irradiation, while CuO_x-anatase shows no activity. Further characterizations showed that visible-light inclines to drive the VB electrons of rutile TiO_2 to CuO_x at the interface between rutile TiO_2 and CuO_x, while it drives the electrons of CuO_x to anatase TiO_2 at interface between anatase TiO_2 and CuO_x. DFT calculations revealed that the interaction between CuO_x and TiO_2 is markedly different in CuO_x-anatase and CuO_x-rutile, which induces the differences in the electronic distribution of interfacial Cu, O and Ti atoms, resulting in the distinct direction of charge transfer.

1. Introduction

TiO_2 is well-known as an efficient photocatalyst, and TiO_2 with different crystalline forms (anatase and rutile) is widely employed to various photocatalytic reactions [1–4]. Owing to the wide band gap, TiO_2 can be only activated under ultraviolet (UV) light irradiation, which limits its practical applications. Nano-copper oxide clusters (CuO_x) grafting is recently shown to be a promising way to expand the visible-light photocatalytic activity of rutile and anatase TiO_2 [5–9]. The CuO_x-TiO_2 has been investigated in many photocatalytic oxidation or reduction, such as degradation of organic pollutants, H_2 evolution, CO_2 reduction, etc. [5–10]. Anatase TiO_2 usually has the higher photocatalytic activity under illumination of UV light compared with rutile TiO_2 due to the wider bandgap and higher surface area [11,12]. Similarly, CuO_x-anatase has also demonstrated the higher activity under UV and visible light compared with CuO_x-rutile [6,10].

On the surface of CuO_x-TiO_2, the photocatalytic reactions are driven by visible-light induced interfacial charge transfer (IFCT) process between CuO_x and TiO_2 [13–15]. Since TiO_2 itself cannot be directly excited by visible light, the electron is usually considered to be excited from the valence band (VB) to conduction band (CB) of CuO_x, and next transfers to the CB of TiO_2, leading to the charge separation [16,17]. Similar scheme was also reported in TiO_2-based heterojunctions, such as CdS-TiO_2, g-C_3N_4-TiO_2, and plasmonic metal-TiO_2 [18,19]. In contrast, several reports have shown that the direct excitation from the VB of TiO_2 to the metal species might occur under visible-light irradiation in the metal-grafted TiO_2 [8,13,17]. Hashimoto et al. reveal that the electrons in the valence band (VB) of rutile phase TiO_2 are excited and migrate to MO_x (for example, CuO_x and FeO_x) through the interface between TiO_2 and MO_x [13]. It is further supported by detecting reaction intermediates, such as trapped holes, trapped electrons, $\cdot O_2^-$, and H_2O_2 [16]. Thus, the direction of the charge migration between CuO_x and TiO_2 is relatively complicated and a further investigation is greatly needed.

In above-mentioned two cases, the generated hole is left in the VB of CuO_x or TiO_2, and the disagreement about the direction of the charge migration on MO_x-TiO_2 should be mainly due to the discrepancy in understanding the origin of the holes. Hence, confirming the location of hole will contribute to the better understanding of charge separation mechanism in CuO_x-TiO_2. Researches usually use decomposition of

* Corresponding authors at: University of Chinese Academy of Sciences, Beijing 100049, PR China.
E-mail addresses: ccchen@iccas.ac.cn (C. Chen), cbzhang@rcees.ac.cn (C. Zhang).

https://doi.org/10.1016/j.apcatb.2021.120735
Received 9 July 2021; Received in revised form 3 September 2021; Accepted 16 September 2021
Available online 20 September 2021

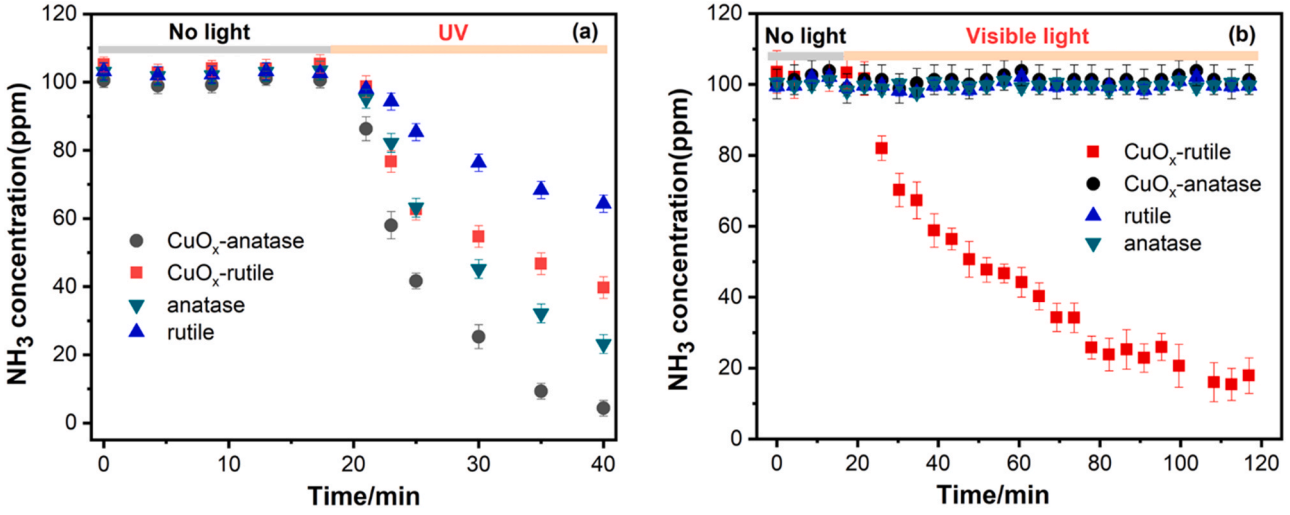

Fig. 1. Photocatalytic oxidation of NH_3 under UV (a) and visible light (b) over different samples. (100 ppm NH_3, 20 vol% O_2, RH 50% and N_2 balance).

model organic pollutants to judge the efficiency of MO_x-TiO_2 [20]. The reported CuO_x-TiO_2 or FeO_x-TiO_2 shows excellent activities for oxidation of acetone and degradation of 2-naphthol or other dyes [16,21]. Since the active species such as holes, electrons, $\cdot O_2^-$, and ·OH are all involved in these reactions, the specific role and source of the hole cannot be determined. Therefore, it is reasonable to propose that a typical oxidation reaction, which is very sensitive to the VB position of a photocatalyst, might be more suitable for effectively investigating the direction of charge migration on MO_x-TiO_2.

Recently, we demonstrated that TiO_2-based hole is the key active species for the oxidation of NH_3 on TiO_2-based photocatalysts, and therefore NH_3 activation can be a good indicator for the presence of TiO_2-based hole [22–24]. In this study, we prepared the CuO_x-grafted rutile and anatase TiO_2 catalysts, and carefully investigated the impact of TiO_2 crystalline structures on the charge migration mechanism of CuO_x-TiO_2 by using a hole position sensitive NH_3 oxidation probe reaction, combining with EPR experiments and DFT calculations. We found that the charge migration pathway of CuO_x-TiO_2 is closely dependent on the crystalline structures of TiO_2, in which at the interface between rutile TiO_2 and CuO_x, visible light drives the VB electrons of rutile TiO_2 to CuO_x, while in case of the interface between anatase TiO_2 and CuO_x, visible light is incline to drive the excitation of CuO_x, and the photoexcited electrons transfer to anatase TiO_2. Our findings about the IFCT process between CuO_x-TiO_2 will be very helpful for the deep understanding of the mechanism of charge migration in MO_x-TiO_2.

2. Experiment

2.1. Synthesis of catalysts

TiO_2 with different crystalline (anatase and rutile) was purchased from Aladdin. 1.0 g anatase or rutile TiO_2 nanoparticles were dispersed into the $CuSO_4$ aqueous solution. The amount of Cu^{2+} relative to the amount of TiO_2 sample was 0.3 wt%. The dispersing solution under stirring was placed into a water-bath kept at 70 °C for 1 h. The obtained precipitates were washed with deionized water several times and then were dried in an oven at 70 °C for 24 h.

2.2. Activity tests

The activity tests for NH_3 oxidation were performed at room temperature in a flow reactor. 0.1 g of photocatalyst powders in a round dish was placed in the center of the reactor. The light source was a 500 W commercial Xe lamp (Beijing TrusTech Science and Technology Co., China). The concentrations of NH_3, NO_x (NO, NO_2) and N_2O were simultaneously measured by an online FTIR (Nicolet IS50) equipped with 2 m gas cell and a DTGS detector, and N_2 selectivity was calculated according to the N element balance by the following equations: N_2 selectivity $= ([NH_3]_{in} - [NO_x]_{out} - 2[N_2O]_{out}) / [NH_3]_{in}$. The reactant gas was 100 ppm NH_3, 20 vol% O_2, RH 50% and N_2 balance. The volume of reactant gas was about 1.5 L.

2.3. Characterization methods

Powder X-ray diffraction (XRD) measurements were performed on a X'Pert PRO MPD X-ray powder diffractometer (Japan) over the 2θ range from 10° to 90° with a scan step size of 0.02°. Transmission electron microscopy (TEM) images of the samples were taken on a JEOL 2100F instrument operating at an accelerating voltage of 200 kV. The UV–vis diffuse reflection spectra (DRS) were tested with UV–vis spectrophotometer (U-3310, Hitachi) using Al_2O_3 as a reference. The X-band electron paramagnetic resonance (EPR) spectra were measured at 90 K using a Bruker E500 EPR spectrometer. The photoelectrochemical measurements were conducted on CHI 630B workstation and a saturated Ag/AgCl electrode and a platinum plate were used as the reference electrode and the counter electrode, respectively.

2.4. Computational methods

The calculations about interaction of CuO_x with the (101) surfaces of anatase or (110) surface of rutile TiO_2 was performed with code VASP. The Perdew-Burke-Ernzerhof (PBE) GGA exchange-correlation functional was applied. A periodic slab with 2 × 2 surface unit cells for (101) surface of anatase TiO_2 and (101) surface of rutile TiO_2 was used. The models contain 108 atoms for (101) facets of anatase TiO_2 and 108 atoms for (110) facets of rutile TiO_2. The bottom two layers of Ti and O were fixed in the process of structure optimization. The vacuum gap thickness was 15 Å. Gamma centered k-point meshes of 2 × 2 × 1 were employed. Structures were relaxed until the forces acting on each atom were smaller than 0.02 eV/Å.

3. Results and discussion

3.1. Activity tests for photocatalytic oxidation of NH_3

The photocatalytic activity for oxidation of NH_3 was firstly tested. As shown in Fig. 1, under UV irradiation, both CuO_x-anatase and CuO_x-rutile show much higher activity compared with pure anatase and rutile

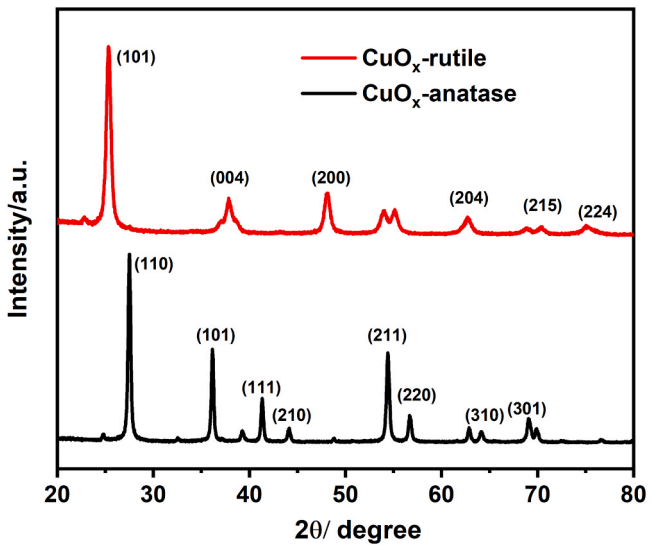

Fig. 2. X-ray diffraction pattern of CuO_x-rutile and CuO_x-anatase.

TiO_2. The CuO_x-anatase is more active than CuO_x-rutile under UV light irradiation (Fig. 1a), and the NH_3 conversion over CuO_x-anatase can reach above 95% in 20 min, while only 60% over CuO_x-rutile. Notably, in the case of visible light irradiation, we surprisingly observed a completely different activity order between CuO_x-rutile and CuO_x-anatase, relative to that of under UV irradiation. The CuO_x-rutile exhibits excellent performance towards NH_3 oxidation, while no any NH_3 conversion is observed at all on CuO_x-anatase (Fig. 1b). We have measured the produced NO_x and N_2O during the reaction over CuO_x-rutile under visible light and the results are presented in Fig. S1. It is shown that no NO and NO_2 was detected and about 12 ppm N_2O is produced, and hence the selectivity of NH_3 to N_2 was calculated to be about 76%. The influences of Cu precursor, Cu loading amount and calcination temperature on the activities of CuO_x-rutile were also investigated (Figs. S2–S4). It is shown that the optimal loading of Cu is 0.3 wt%, and the counterions of the Cu precursors such as chlorine, nitrate and sulfate have no clear impacts on the activity. The drastic different performances between CuO_x-rutile and CuO_x-anatase strongly indicates that there is a distinct mechanism of charge migration on CuO_x-rutile and CuO_x-anatase under visible light irradiation.

3.2. Structural characterizations

The structure of CuO_x-rutile and CuO_x-anatase were next investigated. X-ray diffraction (XRD) analysis shows that CuO_x-anatase and CuO_x-rutile contain the typical anatase and rutile crystalline phases, respectively (Fig. 2). The TEM images display that the CuO_x clusters are uniformly distributed on rutile or anatase TiO_2, and the sizes of the CuO_x clusters in both samples are approximately 1–2 nm (Fig. 3). XPS analysis was employed to further detect the chemical states of the surface CuO_x. As shown in Fig. S5, both CuO_x-anatase and CuO_x-rutile exhibit two peaks of Cu $2p_{1/2}$ (952.9 eV) and Cu $2p_{3/2}$ (933.1 eV), which are assigned to Cu^{2+} [5,25]. We further conducted an EPR experiment to explore the chemical state of CuO_x. The EPR signal with the g factor of 2.394 is dominant on CuO_x-anatase and CuO_x-rutile (Fig. S6), and this signal is ascribed to Cu^{2+} species. Thus, the formed amorphous CuO_x mainly exhibits the state of Cu (II), which is well consistent with the results previously reported [26,27]. Furthermore, the Cu 2p XPS spectra of the CuO_x-rutile and CuO_x-anatase after reaction were also measured. As shown in Figs. S7 and S8, the CuO_x species remained in Cu^{2+} state on the tested samples, indicating that the chemical properties of CuO_x do not change after reaction.

3.3. Photo-electrochemical measurement

The UV–vis diffuse reflectance spectra (DRS) of the rutile TiO_2, CuO_x-rutile, anatase TiO_2 and CuO_x-anatase samples were measured and compared, and the spectra are displayed in Fig. S9. The pristine rutile and anatase TiO_2 show no obvious visible light absorption. After the CuO_x species are grafted, the absorption intensities of both CuO_x-rutile and CuO_x-anatase are increased in the visible light range, indicating that CuO_x clusters on rutile or anatase TiO_2 introduce visible light absorption. To show the origin of the visible light absorption, we further compared the UV–vis diffuse reflectance spectra of CuO_x-rutile and CuO_x-anatase with rutile and anatase TiO_2 as background, respectively. As shown in Fig. 4, CuO_x-rutile has strong absorption in 420–500 nm with a maximum at around 475 nm and 700–800 nm in visible light region, however, the dominant absorption of CuO_x-anatase in visible light region is in the range of 700–800 nm. Evidently, the absorption in 700–800 nm on CuO_x-rutile and CuO_x-anatase stems from the d-d excitation of CuO_x [28]. The absorption of 420–500 nm on CuO_x-rutile should not originate from the individual excitation of TiO_2 or CuO_x, and it may be caused by direct charge transfer from valance band of rutile TiO_2 to CuO_x nanoparticle (see below for more discussion). Other optical properties such as photocurrent and EIS were also measured. Consistent

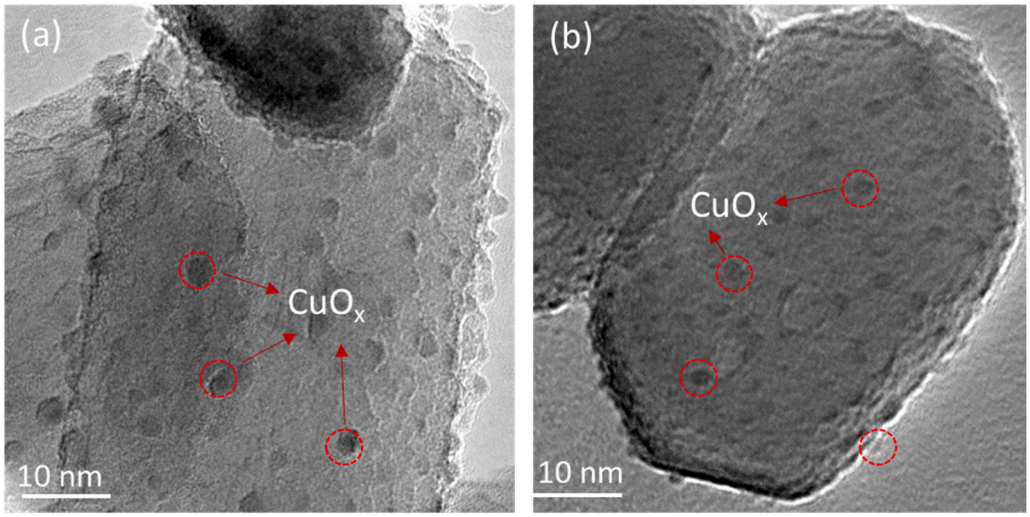

Fig. 3. The TEM image of CuO_x-rutile (a) and CuO_x-anatase (b).

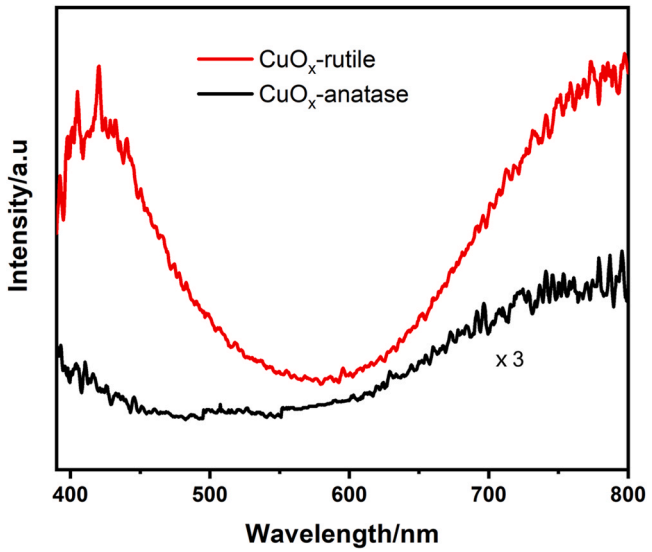

Fig. 4. UV–vis diffuse reflectance spectra of CuO_x-rutile and CuO_x-anatase with rutile and anatase as background, respectively.

with the results about activity tests, the CuO_x-rutile possesses higher photocurrents and the lower electrochemical impedances, compared with CuO_x-anatase under visible light irradiation (Figs. S10 and S11). In contrast, CuO_x-rutile possesses lower photocurrents and the higher electrochemical impedances compared with CuO_x-anatase under UV irradiation (Figs. S12 and S13). These findings further suggest that CuO_x-rutile and CuO_x-anatase may have completely different photoexcitation pathway under visible light.

3.4. Mechanism discussion of charge migration on CuO_x-TiO_2

As reported, the decomposition of model organic pollutants is frequently used to judge the efficiency of CuO_x-TiO_2, for instance, the CuO_x-TiO_2 or FeO_x-TiO_2 shows excellent activities for oxidation of acetone and degradation of 2-naphthol or other dyes [13,29–34]. Since the active species such as holes, electrons, $\cdot O_2^-$, and ·OH are all involved in these reactions, the specific role and source of the hole cannot be determined. Previous studies and our recent reports have confirmed that NH_3 oxidation is a hole-position sensitive reaction, and the activation of NH_3 by hole into NH_2 radical is the activity-determining step [22–24], which means that an active visible-light photocatalyst for NH_3 oxidation should have a low valence band (VB) edge with high oxidation potential. For instance, semiconductor with low VB position, such as TiO_2, Ag_3PO_4, and WO_3, is able to oxidize NH_3 when they are photoexcited under suitable irradiation [23]. The distinct performances in NH_3 oxidation between CuO_x-rutile and CuO_x-anatase suggest that visible light might excites electrons from VB of rutile to the CuO_x, then holes in VB of rutile TiO_2 are capable of oxidizing NH_3. By contrast, visible light might only excite electrons from VB of CuO_x to CB of CuO_x on anatase TiO_2, then holes in VB of CuO_x cannot oxidize NH_3.

EPR is a powerful tool to detect the photo-excited holes and electrons of TiO_2 and to investigate the chemical changes of CuO_x species under UV or visible light irradiation [7,16,28]. Fig. 5 show that the EPR signals of Cu^{2+} in CuO_x-rutile and CuO_x-anatase became broader in the dark, probably due to the inhomogeneity of the chemical structure surrounding Cu^{2+} ions. Upon visible light irradiation, the Cu^{2+} signal decrease in the case of the CuO_x-rutile, and a small signal at $g = 2.010$ ascribed to trapped holes in the VB of TiO_2 is observed. The similar signal is also observed under UV irradiation. However, the Cu^{2+} signal in CuO_x-anatase has no changes upon visible light irradiation, and no signal of trapped holes is observed. When the visible light was switched to UV irradiation, the Cu^{2+} signal on anatase decrease and the signals of trapped holes appear. The decrease of Cu^{2+} signal is associated with the appearance of trapped holes, corresponding to the excited electrons from the VB of TiO_2 to the surface of CuO_x. Hence, we confirm that on the interface of CuO_x and rutile TiO_2, electrons are excited from VB of rutile TiO_2 to the CuO_x under visible light, while in case of the surface of CuO_x and anatase TiO_2, the VB electrons of anatase TiO_2 are not excited under visible light irradiation.

The different photocatalytic charge separation process in semiconductors would induce the formation of distinct reactive species, such as hydroxyl radical (·OH) and superoxide radical ($\cdot O_2^-$), etc. [35,36]. We next measured the related active species on CuO_x-rutile and CuO_x-anatase under visible light. Fig. 6a show that 4 strong characteristic peaks of the DMPO-·OH adducts appear in CuO_x-rutile under visible light, while the DMPO-·OH adducts signal of Cu-anatase is very weak under same conditions, indicating that the large amount of ·OH species are formed on CuO_x-rutile, but it is extremely low on CuO_x-anatase. The $\cdot O_2^-$ species are typical radicals through activating O_2 molecules by the photoexcited electrons [37,38], and the DMPO-$\cdot O_2^-$ species in acetonitrile dispersions were also measured under visible light irradiation (Fig. 6b). Both CuO_x-rutile and CuO_x-anatase has strong DMPO-$\cdot O_2^-$ species signal, indicating electrons from CB of CuO_x or CB of anatase

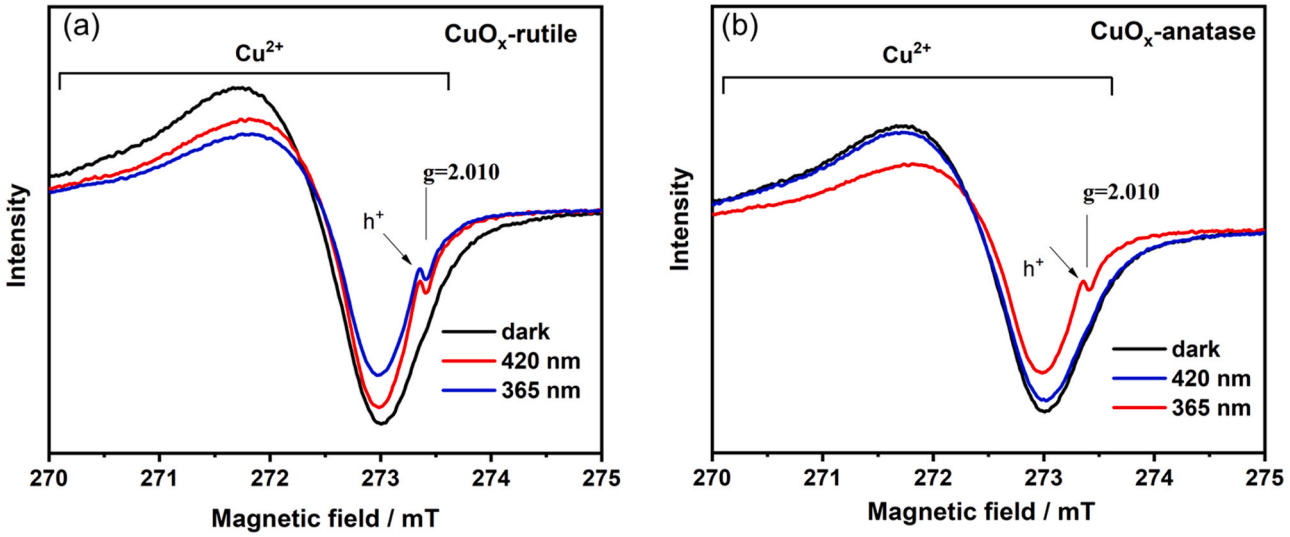

Fig. 5. EPR spectra of CuO_x-rutile (a) and CuO_x-anatase (b) measured at 77 K under vacuum with visible light or UV irradiation.

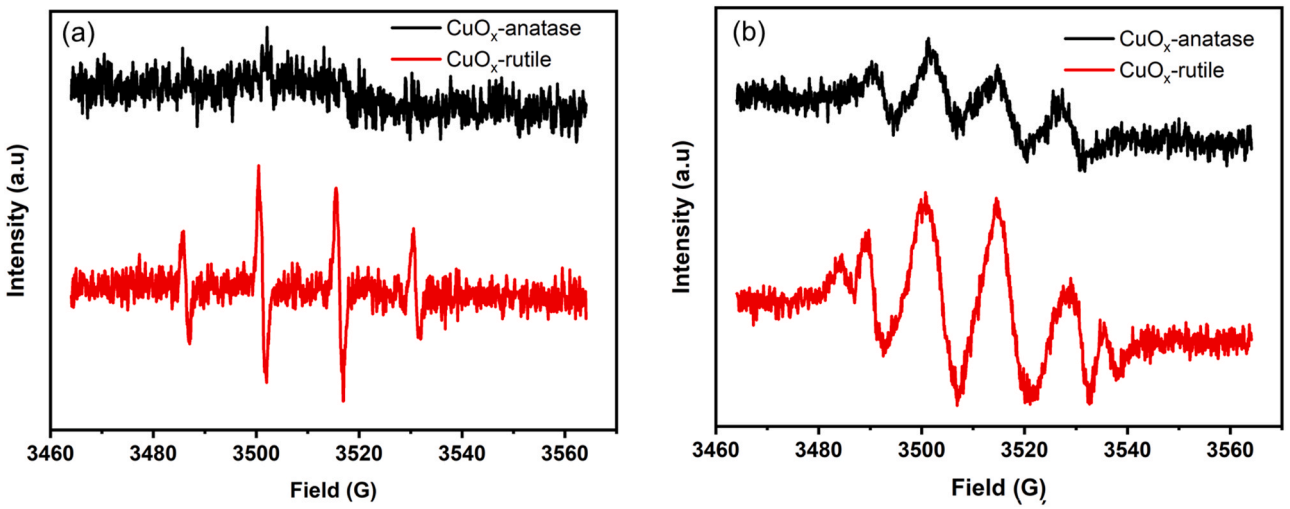

Fig. 6. DMPO spin-trapping EPR spectra measured at 303 K after 5 min visible irradiation in aqueous solutions (a) and acetonitrile (b) over different samples.

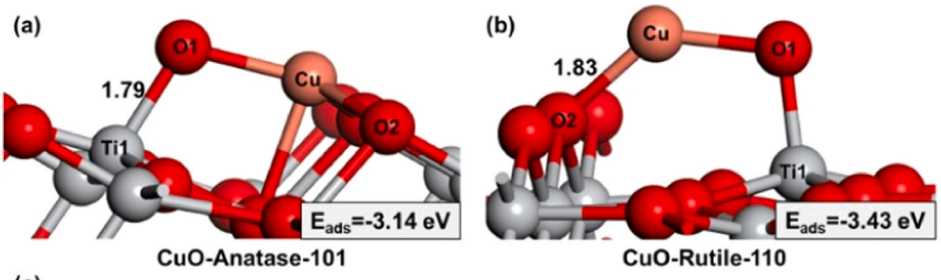

(c)

CuO-Anatase-101	Bader Charge		CuO-Rutile-110	Bader Charge	
	Before adsorption	After adsorption		Before adsorption	After adsorption
Cu	10.40	10.21	Cu	10.37	10.13
O1	6.59	6.77	O1	6.58	6.74
O2	7.00	7.00	O2	6.98	7.08
Ti1	9.86	9.79	Ti1	9.83	9.84

Fig. 7. The optimization structures of CuO-anatase-101 and CuO-rutile-110 (a, b) and Bader charge before and after CuO adsorbed on anatase and rutile (c).

TiO_2 all can efficiently activate O_2. The results of DMPO-·OH adducts and DMPO-·O_2^- adducts further reveal that the sources of excited hole are different on the CuO_x-rutile and CuO_x-anatase under visible light. The holes on CuO_x-rutile are from the low VB of TiO_2, and it is capable of producing the ·OH radicals. In contrast, the holes on CuO_x-anatase are from the VB of CuO_x, and it can not oxidize the H_2O to ·OH radicals.

DFT calculations were next carried out to further explore why charge separation process greatly depend on the crystalline structure of the TiO_2. Fig. 7 presents the optimization structures of CuO-anatase-101 and CuO-rutile-110. It is shown that Cu atom in CuO is bonded with the surface bridge oxygen (O2) of TiO_2, and O1 in CuO is bonded with Ti1 in both CuO-anatase-101 and CuO-rutile-110 interfaces. The interfacial Cu—O2 and Ti1—O1 bonds between CuO and anatase-101 surface have a distance of 2.02 Å and 1.79 Å, while Cu—O2 and Ti—O1 bond between CuO and rutile-110 surface have a distance of 1.83 Å and 1.75 Å. The adsorption energy between CuO_x and different crystalline TiO_2 was then calculated. The adsorption energy is − 3.14 eV and − 3.43 eV for CuO adsorption on anatase and rutile TiO_2, respectively (Fig. 4a), indicating that the interaction between CuO_x and rutile TiO_2 is stronger than that of CuO_x and anatase TiO_2. The Bader charge was further analyzed, and the results are shown in Fig. 4c. When CuO is adsorbed on anatase-101 surface, the Bader charge of interfacial Ti1 is reduced from 9.86 to 9.79, while the Bader charge of the surface bridge oxygen shows no significant change, indicating that the interaction between CuO and anatase is mainly related to the interaction of interfacial Ti and the oxygen in CuO_x. Hence, the interfacial charge transfer between CuO and anatase TiO_2 should occur in the interfacial Ti and the oxygen in CuO_x, specifically, visible light inclines to drive the electrons of interfacial O in CuO_x to the interfacial Ti in anatase-101. Interestingly, in case of CuO-rutile-110, the Bader charge of interfacial Ti has no significant change after CuO adsorb on rutile-110, while the Bader charge of the surface bridge oxygen is increased from 6.98 to 7.08, indicating that the interaction between CuO and rutile TiO_2 mainly stems from the interaction of surface bridge oxygen and interfacial Cu in CuO_x. Therefore, the charge transfer in CuO-rutile-110 takes place in a opposite mode compared with that of CuO-anatase-101, that the visible light inclines to drive the electrons of surface bridge O in rutile-110 to the interfacial Cu in CuO_x.

The strong interaction between noble metal and metal oxide, such as

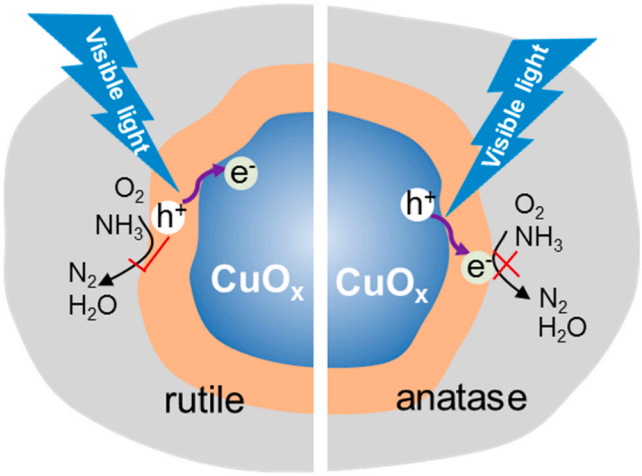

Scheme 1. Charge separation processes in CuO_x-rutile and CuO_x-anatase.

Au, Pt and Pd supported on TiO_2, FeO_x and CeO_2, etc. [39–42], has been widely investigated in the field of catalysis, and it is shown to greatly influence the catalytic activity and selectivity. Additionally, the interface of metal and oxide has been also identified as active site in catalytic oxidation or reduction reactions [43–45]. Our present results show that the interaction between MO_x and TiO_2 is also the key factor determining the direction of charge transfer in CuO_x-TiO_2. Since the interactions between CuO_x and TiO_2 in CuO_x-anatase and CuO_x-rutile are much different from each other, the electronic distributions of interfacial Cu, O and Ti atoms are markedly different, and then inducing the distinct direction of charge transfer.

4. Conclusions

In summary, by using a hole-position sensitive NH_3 oxidation as probe reaction, we found a usual photocatalytic phenomenon that CuO_x-anatase shows better activity than the CuO_x-rutile under UV, and an unusual phenomenon that CuO_x-rutile shows activity, while no activity was observed on CuO_x-anatase under visible light. In combination with EPR and DFT calculations, we discovered that the crystalline forms of TiO_2 remarkably influence the charge separation of CuO_x-TiO_2 due to the different interactions between CuO_x and TiO_2 in CuO_x-anatase and CuO_x-rutile, resulting in the distinct direction of charge transfer. The detailed processes of charge separation are presented in Scheme 1. On the interface of CuO_x and rutile TiO_2, the electrons of rutile TiO_2 are transferred from VB directly to the CuO_x under visible light irradiation. Due to the low VB postion of TiO_2, the left holes have high oxidition potential and therefore could efficiently oxidize NH_3. On the interface of CuO_x and anatase TiO_2, visible light irradiation can only drive the excitation of CuO_x itself. The left holes of CuO_x have low oxidition potential and therefore cannot oxidize NH_3 due to the high VB postion of CuO_x. This work provides a facile probe oxidation reaction to intensively study the mechanism of charge migration in CuO_x-TiO_2 and the findings will contribute to a deeper understanding of the basic photocatalytic process.

CRediT authorship contribution statement

Min Chen: Conceptualization, Methodology, Validation, Formal analysis, Investigation, Resources, Data curation, Visualization, Writing – original draft, Writing – review & editing. **Jianhua Chen:** Investigation, Resources, Data curation. **Chuncheng Chen:** Formal analysis, Investigation, Writing – original draft. **Changbin Zhang:** Writing – original draft, Writing – review & editing, Supervision, Project administration, Funding acquisition. **Hong He:** Supervision, Project administration.

Declaration of Competing Interest

The authors declare that they have no known competing financial interests or personal relationships that could have appeared to influence the work reported in this paper.

Acknowledgements

This work was financially supported by the National Key Research and Development Program of China (2017YFC0211802) and the National Natural Science Foundation of China (21906174, 22025604, 21976196).

Appendix A. Supporting information

Supplementary data associated with this article can be found in the online version at doi:10.1016/j.apcatb.2021.120735.

References

[1] A. Fujishima, X.T. Zhang, D.A. Tryk, TiO_2 photocatalysis and related surface phenomena, Surf. Sci. Rep. 63 (2008) 515–582.
[2] H. Xu, S. Ouyang, L. Liu, P. Reunchan, N. Umezawa, J. Ye, Recent advances in TiO_2-based photocatalysis, J. Mater. Chem. A 2 (2014) 12642–12661.
[3] R. Asahi, T. Morikawa, H. Irie, T. Ohwaki, Nitrogen-doped titanium dioxide as visible-light-sensitive photocatalyst: designs, developments, and prospects, Chem. Rev. 114 (2014) 9824–9852.
[4] J. Low, B. Cheng, J. Yu, Surface modification and enhanced photocatalytic CO_2 reduction performance of TiO_2: a review, Appl. Surf. Sci. 392 (2017) 658–686.
[5] S. Zhu, X.F. Chen, Z.C. Li, X.Y. Ye, Y. Liu, Y. Chen, L. Yang, M. Chen, D.Q. Zhang, G. S. Li, H.X. Li, Cooperation between inside and outside of TiO_2: lattice Cu^+ accelerates carrier migration to the surface of metal copper for photocatalytic CO_2 reduction, Appl. Catal. B: Environ. 264 (2020), 118515.
[6] D.W. Ni, H.Y. Shen, H.Q. Li, Y. Ma, T.Y. Zhai, Synthesis of high efficient Cu/TiO_2 photocatalysts by grinding and their size-dependent photocatalytic hydrogen production, Appl. Surf. Sci. 409 (2017) 241–249.
[7] N. Seriani, C. Pinilla, Y. Crespo, Presence of gap states at Cu/TiO_2 anatase surfaces: consequences for the photocatalytic activity, J. Phys. Chem. C 119 (2015) 6696–6702.
[8] K. Osako, K. Matsuzaki, T. Susaki, S. Ueda, G. Yin, A. Yamaguchi, H. Hosono, M. Miyauchi, Direct observation of interfacial charge transfer between rutile TiO_2 and ultrathin CuO_x Film by visible-light illumination and its application for efficient photocatalysis, Chemcatchem 10 (2018) 3666–3670.
[9] A. Šuligoj, I. Arčon, M. Mazaj, G. Dražić, D. Arčon, P. Cool, U.L. Štangar, N. N. Tušar, Surface modified titanium dioxide using transition metals: nickel as a winning transition metal for solar light photocatalysis, J. Mater. Chem. A 6 (2018) 9882–9892.
[10] P. Unwiset, A. Makdee, K.C. Chanapattharapol, P. Kidkhunthod, Effect of Cu addition on TiO_2 surface properties and photocatalytic performance: X-ray absorption spectroscopy analysis, J. Phys. Chem. Solids 120 (2018) 231–240.
[11] Y. Ide, N. Inami, H. Hattori, K. Saito, M. Sohmiya, N. Tsunoji, K. Komaguchi, T. Sano, Y. Bando, D. Golberg, Y. Sugahara, Remarkable charge separation and photocatalytic efficiency enhancement through interconnection of TiO_2 nanoparticles by hydrothermal treatment, Angew. Chem. Int. Ed. 55 (2016) 3600–3605.
[12] G. Xiang, Y.G. Wang, D. Wu, T. Li, J. He, J. Li, X. Wang, Size-dependent surface activity of rutile and anatase TiO_2 nanocrystals: facile surface modification and enhanced photocatalytic performance, Chemistry 18 (2012) 4759–4765.
[13] H. Irie, K. Kamiya, T. Shibanuma, S. Miura, D.A. Tryk, T. Yokoyama, K. Hashimoto, Visible light-sensitive Cu (II)-grafted TiO_2 photocatalysts: activities and X-ray absorption fine structure analyses, J. Phys. Chem. C 113 (2009) 10761–10766.
[14] D. Wang, X.Y. Pan, G.T. Wang, Z.G. Yi, Improved propane photooxidation activities upon nano Cu_2O/TiO_2 heterojunction semiconductors at room temperature, RSC Adv. 5 (2015) 22038–22043.
[15] M.V. Dozzi, G.L. Chiarello, M. Pedroni, S. Livraghi, E. Giamello, E. Selli, High photocatalytic hydrogen production on Cu (II) pre-grafted Pt/TiO_2, Appl. Catal. B 209 (2017) 417–428.
[16] Y. Nosaka, S. Takahashi, H. Sakamoto, A.Y. Nosaka, Reaction mechanism of Cu (II)-grafted visible-light responsive TiO_2 and WO_3 photocatalysts studied by means of ESR spectroscopy and chemiluminescence photometry, J. Phys. Chem. C 115 (2011) 21283–21290.
[17] Q. Jin, M. Fujishima, A. Iwaszuk, M. Nolan, H. Tada, Loading effect in copper (II) oxide cluster-surface-modified titanium (IV) oxide on visible- and UV-light activities, J. Phys. Chem. C 117 (2013) 23848–23857.
[18] D. Zhang, Y.L. Guo, Z.K. Zhao, Porous defect-modified graphitic carbon nitride via a facile one-step approach with significantly enhanced photocatalytic hydrogen evolution under visible light irradiation, Appl. Catal. B 226 (2018) 1–9.
[19] J. Yu, S. Wang, J. Low, W. Xiao, Enhanced photocatalytic performance of direct Z-scheme g-C_3N_4-TiO_2 photocatalysts for the decomposition of formaldehyde in air, Phys. Chem. Chem. Phys. 15 (2013) 16883–16890.

[20] C.C. Chen, W.H. Ma, J.C. Zhao, Semiconductor-mediated photodegradation of pollutants under visible-light irradiation, Chem. Soc. Rev. 39 (2010) 4206–4219.
[21] M. Liu, X. Qiu, M. Miyauchi, K. Hashimoto, Energy-level matching of Fe (III) ions grafted at surface and doped in bulk for efficient visible-light photocatalysts, J. Am. Chem. Soc. 135 (2013) 10064–10072.
[22] M. Chen, J.Z. Ma, B. Zhang, G.Z. He, Y.B. Li, C.B. Zhang, H. He, Remarkable synergistic effect between {001} facets and surface F ions promoting hole migration on anatase TiO_2, Appl. Catal. B 207 (2017) 397–403.
[23] M. Chen, C. Zhang, H. He, Insights into designing photocatalysts for gaseous ammonia oxidation under visible light, Environ. Sci. Technol. 54 (2020) 10544–10550.
[24] M. Chen, J.Z. Ma, B. Zhang, F. Wang, Y.B. Li, C.B. Zhang, H. He, Facet-dependent performance of anatase TiO_2 for photocatalytic oxidation of gaseous ammonia, Appl. Catal. B 223 (2018) 209–215.
[25] G.Q. Cao, N.A. Deskins, N. Yi, Chemical source profiles of particulate matter and gases emitted from solid fuels for residential cooking and heating scenarios in Qinghai-Tibetan Plateau, Environ. Pollut. 285 (2021), 117503.
[26] Y.J. Kim, J.K. Lee, K.M. Min, S.B. Hong, I.-S. Nam, B.K. Cho, Hydrothermal stability of CuSSZ-13 for reducing NO_x by NH_3, J. Catal. 311 (2014) 447–457.
[27] L. Liu, F. Gao, H. Zhao, Y. Li, Tailoring Cu valence and oxygen vacancy in Cu/TiO_2 catalysts for enhanced CO_2 photoreduction efficiency, Appl. Catal. B. 134–135 (2013) 349–358.
[28] M. Jung, J.N. Hart, J. Scott, Y.H. Ng, Y. Jiang, R. Amal, Exploring Cu oxidation state on TiO_2 and its transformation during photocatalytic hydrogen evolution, Appl. Catal. A 521 (2016) 190–201.
[29] M.H. Jeong, J. Sun, G.Y. Han, D.H. Lee, J.W. Bae, Successive reduction-oxidation activity of FeO_x/TiO_2 for dehydrogenation of ethane and subsequent CO_2 activation, Appl. Catal. B: Environ. 270 (2020), 118887.
[30] H. Zhang, W. Wang, H. Zhao, L. Zhao, L.-Y. Gan, L.-H. Guo, Facet-dependent interfacial charge transfer in Fe (III)-grafted TiO_2 nanostructures activated by visible light, ACS Catal. 8 (2018) 9399–9407.
[31] H. Yu, H. Irie, Y. Shimodaira, Y. Hosogi, Y. Kuroda, M. Miyauchi, K. Hashimoto, An efficient visible-light-sensitive Fe (III)-grafted TiO_2 photocatalyst, J. Phys. Chem. C 114 (2010) 16481–16487.
[32] X. Qiu, M. Miyauchi, H. Yu, H. Irie, K. Hashimoto, Visible-light-driven Cu (II)-$(Sr_{1-y}Na_y)(Ti_{1-x}Mo_x)O_3$ photocatalysts based on conduction band control and surface ion modification, J. Am. Chem. Soc. 132 (2010) 15259–15267.
[33] Y. Li, W.-N. Wang, Z. Zhan, M.-H. Woo, C.-Y. Wu, P. Biswas, Photocatalytic reduction of CO_2 with H_2O on mesoporous silica supported Cu/TiO_2 catalysts, Appl. Catal. B 100 (2010) 386–392.
[34] N. Murakami, T. Chiyoya, T. Tsubota, T. Ohno, Switching redox site of photocatalytic reaction on titanium (IV) oxide particles modified with transition-metal ion controlled by irradiation wavelength, Appl. Catal. A 348 (2008) 148–152.
[35] S.L. Wang, X. Luo, X. Zhou, Y. Zhu, X. Chi, W. Chen, K. Wu, Z. Liu, S.Y. Quek, G. Q. Xu, Fabrication and properties of a free-standing two-dimensional titania, J. Am. Chem. Soc. 139 (2017) 15414–15419.
[36] S.-J. Yuan, J.-J. Chen, Z.-Q. Lin, W.-W. Li, G.-P. Sheng, H.-Q. Yu, Nitrate formation from atmospheric nitrogen and oxygen photocatalysed by nano-sized titanium dioxide, Nat. Commun. 4 (2013) 2249.
[37] M. D'Arienzo, J. Carbajo, A. Bahamonde, M. Crippa, S. Polizzi, R. Scotti, L. Wahba, F. Morazzoni, Photogenerated defects in shape-controlled TiO_2 anatase nanocrystals: a probe to evaluate the role of crystal facets in photocatalytic processes, J. Am. Chem. Soc. 133 (2011) 17652–17661.
[38] M.M. Montemore, M.A. van Spronsen, R.J. Madix, C.M. Friend, O_2 activation by metal surfaces: implications for bonding and reactivity on heterogeneous catalysts, Chem. Rev. 118 (2018) 2816–2862.
[39] J. Resasco, L. DeRita, S. Dai, J.P. Chada, M. Xu, X. Yan, J. Finzel, S. Hanukovich, A. S. Hoffman, G.W. Graham, S.R. Bare, X. Pan, P. Christopher, Uniformity is key in defining structure-function relationships for atomically dispersed metal catalysts: the case of Pt/CeO_2, J. Am. Chem. Soc. 142 (2020) 169–184.
[40] B. Han, Y. Guo, Y. Huang, W. Xi, J. Xu, J. Luo, H. Qi, Y. Ren, X. Liu, B. Qiao, T. Zhang, Strong metal-support interactions between Pt single atoms and TiO_2, Angew. Chem. Int. Ed. 59 (2020) 11824–11829.
[41] H. Wang, J.X. Liu, L.F. Allard, S. Lee, J. Liu, H. Li, J. Wang, J. Wang, S.H. Oh, W. Li, M. Flytzani-Stephanopoulos, M. Shen, B.R. Goldsmith, M. Yang, Surpassing the single-atom catalytic activity limit through paired Pt-O-Pt ensemble built from isolated Pt1 atoms, Nat. Commun. 10 (2019) 3808.
[42] D. Kunwar, S. Zhou, A. DeLaRiva, E.J. Peterson, H. Xiong, X.I. Pereira-Hernández, S.C. Purdy, R. ter Veen, H.H. Brongersma, J.T. Miller, H. Hashiguchi, L. Kovarik, S. Lin, H. Guo, Y. Wang, A.K. Datye, Stabilizing high metal loadings of thermally stable platinum single atoms on an industrial catalyst support, ACS Catal. 9 (2019) 3978–3990.
[43] M. Cargnello, V.V. Doan-Nguyen, T.R. Gordon, R.E. Diaz, E.A. Stach, R.J. Gorte, P. Fornasiero, C.B. Murray, Control of metal nanocrystal size reveals metal-support interface role for ceria catalysts, Science 341 (2013) 771–773.
[44] G. Chen, Y. Zhao, G. Fu, P.N. Duchesne, L. Gu, Y. Zheng, X. Weng, M. Chen, P. Zhang, C.W. Pao, J.F. Lee, N. Zheng, Interfacial effects in iron-nickel hydroxide-platinum nanoparticles enhance catalytic oxidation, Science 344 (2014) 495–499.
[45] Y.-Q. Su, Y. Wang, J.-X. Liu, I.A.W. Filot, K. Alexopoulos, L. Zhang, V. Muravev, B. Zijlstra, D.G. Vlachos, E.J.M. Hensen, Theoretical approach to predict the stability of supported single-atom catalysts, ACS Catal. 9 (2019) 3289–3297.